

Lidar Data Remote Sensing Of Aerosols And Anisotropic Space-Time Generalizations Of Corrsin-Obukov And Kolmogorov Laws

A. Radkevich¹, S. Lovejoy^{1*}, K.B. Strawbridge², D. Schertzer³

¹Department of Physics, McGill University, 3600 University st., Montreal, Que., Canada

²Meteorological Service of Canada, Experimental Studies Division, Centre for Atmospheric Research Experiments (CARE), 6248 Eighth Line, Egbert, Ontario L0L 1N0

³CEREVE, Ecole Nationale des Ponts et Chaussées, 6-8, avenue Blaise Pascal, Cité Descartes, 77455 MARNE-LA-VALLEE Cedex, France

ABSTRACT

In this paper we concentrate on the space-time behaviour of atmospheric passive scalars. We first recall that – although the full (x, y, z, t) turbulent processes respect an anisotropic scale invariance, that due to advection, the generator will generally not be a diagonal matrix. This implies that the scaling of (1D) temporal series will generally involve three exponents in real space: $1/3$, $1/2$, $3/5$; for spectra $\beta_\tau = 5/3$, 2 , $11/5$ with the first and last corresponding to domination by advection (horizontal and vertical respectively), and the middle to pure temporal development. We survey the literature and find that almost all the empirical results indeed have β_τ in the range $5/3$ or 2 (the $11/5$ value requires apparently unrealistic vertical winds). We then use state-of-the-art vertically pointing lidar data of backscatter ratios from both aerosols and cirrus clouds yielding several (z, t) vertical space - time cross-sections with resolution of 3.75 m in the vertical, 0.5 s - 30 s in time and spanning 3-4 orders of magnitude in temporal scale.

We first tested the predictions of the anisotropic, multifractal extension of the Corrsin-Obukhov law in the vertical and in time separately finding that the cirrus and aerosols both followed the theoretical (anisotropic) scalings accurately; most (but not all) of the cases showed a dominance by the horizontal wind. In order to test the theory in arbitrary directions in this (z, t) space, and in order to get more complete information about the underlying physical scale, we developed and applied a new Anisotropic Scaling Analysis Technique (ASAT) which is based on a nonlinear space-time coordinate transformation. This transforms the original differential scaling into standard self-similar scaling; there remains only a “trivial” anisotropy. This method was used in real space on 2D structure functions as well as in fourier space on spectral densities. It was applied to both the (z, t) data as well as the (x, z) data discussed in [Lilley *et al* 2004] Using the ASAT technique we verified the theory to within about 10% over more than 3 orders of magnitude of space-time scales in arbitrary directions in (x, z) and (z, t) spaces. By considering the high (and low) order structure functions, we verify the theory for both weak and strong structures (as predicted, their average anisotropies are apparently the same).

Putting together the results for (x, z) and (z, t) (and assuming that there is no overall stratification in the horizontal (x, y) plane), we find that the overall (x, y, z, t) space is found to have an “elliptical dimension” characterizing the overall space-time stratification equal to $D_{st}=3.21\pm 0.05$ which is close to the theoretical value $D_{st}=1+1+5/9+2/3=29/9=3.22\dots$ corresponding (in conditions with no mean wind) to $k_x^{-5/3}$, $k_y^{-5/3}$, $k_z^{-11/5}$ scaling in space and ω^{-2} scaling in time.

* Corresponding author: Department of Physics, McGill University, 3600 University st., Montreal, QC, Canada, H3A 2T8,
e-mail: lovejoy@physics.mcgill.ca

1. INTRODUCTION

To date, the great majority of turbulence theories have postulated *a priori* that all the relevant regimes are isotropic. They thus require at least two regimes to model the atmosphere: a (quasi) two dimensional isotropic large scale and (quasi) three dimensional isotropic small scale. Since the scale height H_s for the mean pressure is about 7.5 km, the “dimensional transition” from isotropic 2D to isotropic 3D turbulence must occur somewhere in the meso-scale; this is the origin of the elusive “meso-scale gap” in the energy spectrum which we discuss below. The main exceptions to isotropic scaling (“self-similar”) theories are the weakly nonlinear gravity wave theories (see Dewan and Good (1986), Dewan (1997), Gardner (1994) and review in Lovejoy *et al.* (2006)) and the 23/9 D anisotropic “unified scaling” model proposed in (Schertzer and Lovejoy 1985). Stochastic multifractal models following this scaling symmetry and obeying the multifractal extensions of the Kolmogorov and Corrsin-Obukhov statistics were proposed in (Schertzer and Lovejoy 1987); the Fractionally Integrated Flux (FIF) model. These involve the notion of scaling stratification and are the main focus of this three part paper.

To understand the meaning of scaling stratification, consider the dimension which characterizes the stratification. In a 2D atmosphere, there is only variability in the horizontal direction. In a 3D atmosphere, if x and z are horizontal and vertical and $\Delta\rho(\Delta x, 0, 0)$ designates density fluctuations in the horizontal and vertical directions over separation Δx , Δz then if the variability is statistically isotropic - on average (“ $\langle \rangle$ ”) $\langle |\Delta\rho(\Delta x, 0, 0)| \rangle = \langle |\Delta\rho(0, 0, \Delta z)| \rangle$. In an intermediate ($2 < D < 3$) stratified but still scaling case, we need only go a distance $(\Delta z/l_s) = (\Delta x/l_s)^{H_z}$ with $0 < H_z < 1$ to find that $\langle |\Delta\rho(\Delta x, 0, 0)| \rangle = \langle |\Delta\rho(0, 0, \Delta z)| \rangle$. We see that $H_z = 1$ corresponds to 3D isotropy and $H_z = 0$ to 2D (isotropy in the horizontal plane; thickness independent of horizontal extend). The dimensional parameter l_s – the “sphero-scale” is the scale at which going a distance $\Delta x = \Delta z = l_s$ yields the same fluctuations: $\langle |\Delta\rho(l_s, 0, 0)| \rangle = \langle |\Delta\rho(0, 0, l_s)| \rangle$. In scaling stratification, the aspect ratio of structures in vertical cross-sections therefore varies as a power law of scale; in addition, (assuming horizontal isotropy, i.e. $\Delta y \approx \Delta x$) the volume of typical structures varies as $\Delta x \Delta x \Delta x^{H_z} = \Delta x^{D_s}$ with $D_s = 2 + H_z$. The intermediate dimension D_s is called

an “elliptical dimension” because of the typical elliptical shapes of the vertical sections of the average structures. Note that the notion of dimension can also be used in a rather different sense to characterize the intermittency of this stratified turbulence. The elliptical dimension is a trace of the generator of the group of scale change operators (see below). As we shall see below, the proposal by (Schertzer & Lovejoy 1983b, 1985a, 1985b) that horizontal structures are dominated by energy fluxes, while vertical structures are dominated by buoyancy variance fluxes implies $H_z = 5/9$ and hence $D_s = 23/9$ (the “s” indicates “space”; below we consider the extension to space-time).

Since each of the above atmospheric models implies a specific elliptical dimension D_s (or equivalently, H_z) it ought to be straightforward to empirically test them simply by measuring D_s (or H_z) over the relevant ranges. The difficulty has been that until recently, tests have primarily been made using either aircraft wind data in the horizontal or balloon wind data in the vertical (the exception is (Lilley *et al.* 2004); lidar vertical cross-sections, see below and Lilley *et al.* (2006)). The results from separate experiments often from different parts of the world and under different conditions, can only be compared in an indirect way (with the partial exception of (Chigirinskaya *et al.* 1994), Lazarev *et al.* 1994). An additional problem is that aircraft do not fly in perfectly flat trajectories nor do balloons rise in perfect vertical paths so that in-situ wind velocity, temperature or density measurements made with such means can only be made over irregular trajectories. Indeed, it has only recently (Lovejoy *et al.* 2004) been discovered that – precisely due to non 2D turbulence - aircraft can follow fractal trajectories (i.e. can be biased with respect to linear trajectories over large distances). Therefore, such in-situ data can yield spurious statistical exponents, spurious scaling breaks and erroneous interpretations. Finally, huge amounts of data are needed in order to average over the large fluctuations in order to obtain accurate results (Lilley *et al.* (2004, 2006)).

In a recent paper Lilley (2004, 2006) it was argued that an anisotropic multifractal extension of the classical Corrsin-Obukhov law for passive scalars gives an accurate description of the horizontal stratification of the atmosphere including its intermittency. In (Lovejoy *et al.* 2006) we also argued that by extending this further to anisotropic space-time, the overall result could be used as the basis for a turbulence/wave model in which spatially and temporally localized turbulent fluxes provide the sources for unlocalized velocity and density fluctuations. This model was based on an energy flux dominating the horizontal and a

buoyancy force variance flux dominating the vertical (both of which are quadratic invariants and hence should be conserved scale by scale). In contrast to the main gravity wave models - which require a weakly nonlinear state in order to justify the use of linear dispersion relations - this model assumes that the atmosphere is highly heterogeneous and turbulent.

In Lilley (2004) airborne lidar data were used to test a key quantitative difference between the gravity wave and turbulence wave models: the stratification of space (x, y, z) is characterized by $D_s = 1+1+1/3=7/3$ in the former, whereas in the latter by $D_s = 1+1+5/9=23/9$. Since we found empirically from vertical cross-sections of lidar backscatter ratio that $D_s = 2.55 \pm 0.02$, the evidence was firmly in favour of the turbulence/wave model. However, the model predicted the full space-time statistical scaling behaviour: it uses classical Kolmogorov type arguments to argue that for the full space-time domain (x, y, z, t) , $D_{st} = 23/9+2/3=29/9$. For more full space-time validation of the model, we must turn to the time domain. In this paper, we therefore seek to extend the vertical (x, z) analyses to space-time (z, t) analyses.

2. TEMPORAL SCALING IN THE ATMOSPHERE

2.1 Theoretical considerations

Following the classical Kolmogorov approach, we may obtain the scaling law for horizontal and temporal velocity fluctuations using dimensional analysis based on the fact that the nonlinear terms of the Navier-Stokes equations conserve energy fluxes. The idea is that there is a quasi-steady energy flux input from large scales balanced (on average only) by kinetic energy dissipation at small scales. Since the kinetic energy flux (per unit of mass) across an eddy (structure) with shear Δv is $\varepsilon = \Delta v^2 / \tau$, we need only estimate the characteristic time for the transfer, τ . For fluctuations in the horizontal, the only time scale available is $\tau = \Delta x / \Delta v \Rightarrow \Delta v = \varepsilon^{1/3} \Delta x^{H_h}$ with $H_h = 1/3$ which is the familiar Kolmogorov result (in Fourier space, the corresponding isotropic energy spectrum - ignoring intermittency - is $E(k) \approx k^{-\beta_h}$; $\beta_h = 1+2H_h = 5/3$).

In time, there are two classical approaches to estimating the fluctuations. The first is to consider a Lagrangian framework (following the mean flow); dimensional analysis yields $H_\tau = 1/2$ (Inoue 1951, Landau and Lifshitz 1959); this gives spectral exponent $\beta_\tau = 1+2H_\tau = 2$. In cases where there is a very low mean velocity, the Eulerian (fixed frame) is equivalent so that in this case of "pure" temporal development, we expect $H_\tau = 1/2$. At the other extreme, if the turbulence is blown past with mean velocity U so quickly that it is practically "frozen" (i.e. it satisfies the conditions of Taylor's 1938 "frozen turbulence" hypothesis), then we can use the horizontal law but with $\Delta x = U \Delta t$ so that: $\Delta v = \varepsilon^{1/3} U^{1/3} \Delta t^{H_t}$ with $H_\tau = 1/3$ (hence $\beta_t = 1+2H_\tau = 5/3$). Using scale functions, and appealing to the Galilean invariance of the governing fluid equations, (Schertzer *et al.* 1998) we show more generally how to take both arbitrary advection and pure temporal development into account in a single equation which is an anisotropic and multifractal generalization of the classical Kolmogorov law:

$$\Delta v(\Delta \mathbf{R}) = \varepsilon_{[\Delta \mathbf{R}]}^{1/3} [[\Delta \mathbf{R}]]^{1/3} \quad (1a)$$

where $\Delta \mathbf{R} = (\Delta x, \Delta y, \Delta z, \Delta t)$ and $[[\Delta \mathbf{R}]]$ is a space-time scale function respecting the scale equation: with $G' = A^{-1}GA$ where G is a diagonal matrix with diagonal elements $1, 1, H_z, H_t$ ($H_z = 5/9, H_t = 2/3$) and A is the Galilean transformation matrix:

$$A = \begin{pmatrix} 1 & 0 & 0 & -v_x \\ 0 & 1 & 0 & -v_y \\ 0 & 0 & 1 & -v_z \\ 0 & 0 & 0 & 1 \end{pmatrix} \quad (1b)$$

where $\mathbf{v} = (v_x, v_y, v_z)$ is the advection velocity. Using the simplest "canonical scale function":

$$[[\Delta \mathbf{r}, \Delta t]]_{can} = l_s \left[\left(\frac{\Delta x - v_x \Delta t}{l_s} \right)^2 + \left(\frac{\Delta y - v_y \Delta t}{l_s} \right)^2 + \left(\frac{\Delta z - v_z \Delta t}{l_s} \right)^{2/H_z} + \left(\frac{\Delta t}{\tau_s} \right)^{2/H_t} \right] \quad (1c)$$

Where $\Delta \mathbf{r} = (\Delta x, \Delta y, \Delta z)$ and the sphero-scale $l_s = \phi^{-3/4} \varepsilon^{5/4}$ and sphero-time $\tau_s = \phi^{-1/2} \varepsilon^{1/2}$ is the eddy turn over time (lifetime) at the sphero-scale (in a heterogeneous turbulent atmosphere it is the analogue of the inverse Brunt-Väisälä frequency). For temporal fluctuations at a point (i.e.

$\Delta \mathbf{r} = (0, 0, 0)$) we obtain the statistics of the pure temporal fluctuations:

$$\Delta v(0, 0, 0, \Delta t) = \varepsilon^{1/2} \tau_s^{1/2} \times \left[\left(\frac{v_x \Delta t}{l_s} \right)^2 + \left(\frac{v_y \Delta t}{l_s} \right)^2 + \left(\frac{v_z \Delta t}{l_s} \right)^{2/H_z} + \left(\frac{\Delta t}{\tau_s} \right)^{2/H_t} \right]^{1/6} \quad (2)$$

$$H_z = 5/9, \quad H_t = 2/3$$

See section 3 for the extension to passive scalar advection, to general $\Delta \mathbf{R}$ and more general scale functions. This reduces to the classical Lagrangian frame result when $\mathbf{v} = (0, 0, 0)$. When the horizontal velocity term is dominant this reduces to the “Frozen turbulence” result (although the turbulence is only statistically “frozen”). The precise condition for this is when $(v \Delta t / l_s)^2 > (\Delta t / \tau_s)^3$ (where the speed $v = \left(v_x^2 + v_y^2 + 0 \right)^{1/2}$); this is equivalent to: $\Delta t < \tau_s (v / v_s)^2$. Using the dimensional analysis values for the sphero scale l_s and sphero-time τ_s above, we find that the condition the velocity term dominates for short times is $\Delta t < v^2 / \varepsilon$, so that the cut-off is shorter for low advection velocities or for high levels of turbulence. Due to the huge fluctuations in energy flux, this limit will be extremely variable, - in fact if the analyses of (Lilley *et al.* 2006) are correct, then $\langle \varepsilon^{-1} \rangle$ diverges (since $\alpha < 2$) - a

consequence of the fact that for Log Levy distributions, ε often takes values near zero. An analogous analysis can be made of the vertical term: taking $H_z = 5/9$ and putting $v_x = v_y = 0$, we find that the vertical velocity can only dominate for the very long times satisfying: $\Delta t > \phi^{-2} \varepsilon^5 v_z^{-6}$.

However since v_z is typically small, this time for dominance may be quite long (perhaps so long that it is never observed). In summary, we have:

$$\begin{aligned} H_\tau &= 1/3; & \beta_\tau &= 5/3; & \Delta t &< v^2 \varepsilon^{-1} \\ H_\tau &= 1/2; & \beta_\tau &= 2; & v^2 \varepsilon^{-1} &< \Delta t < \phi^{-2} \varepsilon^5 v_z^{-6} \\ H_\tau &= 3/5; & \beta_\tau &= 11/5; & \phi^{-2} \varepsilon^5 v_z^{-6} &< \Delta t \end{aligned} \quad (3)$$

(where we have omitted the relatively small intermittency corrections in the β estimates). We conclude that there will be many cases when the $H_\tau = 1/2$ pure temporal development exponent will not be visible due to advection in either horizontal or vertical directions.

2.2 Review of the empirical evidence

The prediction that the time exponent would typically be either 5/3 or 2 – and possibly 11/5 – is in accord with many of the observations surveyed in (Lilley *et al.* 2004), the main gravity wave theories assume $\beta_\tau = 2$ (the saturated cascade theory) or β_t in the range 5/3 to 2 (the exact value is not so important) in the Diffusive Filtering Theory. The experimental literature confirms two possible temporal exponents $\beta_t = 5/3$ and $\beta_\tau = 2$ (see table 1 for review of experimental literature).

Table 1. Review of empirical evidence of temporal power laws $-5/3$ and -2 for wind, passive scalars.

| Author and Year | Experimental Technique | Quantity measured | Observations made by author | Frequency range, Hz | Spectral Exponent β measured |
|---|--|--|--|--|---|
| Hwang ^{a)} (1971) | Anemometers of the three-cup generator and counter types | Wind speed | Atmospheric turbulence followed $-5/3$ power law | 3×10^{-7} - 1×10^{-4} 1×10^{-5} - 6×10^{-2} | Reference slope of $-5/3$ is shown |
| Balsley and Carter ^{b)} (1982) | MST radar | Horizontal wind speed at the altitudes 8 km and 86 km | The resulting curve corresponds very well to an $\omega^{-5/3}$ slope out to the high frequency limit | 3×10^{-3} - 1×10^{-7} 6×10^{-3} - 4×10^{-7} | Reference slope of $-5/3$ is shown |
| Larsen <i>et al.</i> ^{c)} (1982) | MST radar | Horizontal wind speed at several altitudes from 6 to 15 km | Spectra follow $-5/3$ power law in the range of periods from 2 to 50 h. Refer to Taylor's transformation and $-5/3$ power law for horizontal wave number | 3×10^{-7} - 3×10^{-4} | Exponents from -1.24 to -2 are obtained depending on wind component and altitude |
| Scheffler and Liu ^{d)} (1985) | MST radar | Horizontal wind speed | Acoustic Gravity wave theory proposed that "quantitatively relates the MST radar observed wind fluctuation spectrum | 2×10^{-5} - 2×10^{-2} | Slope of -2 fits data very well |
| Balsley and Garelo ^{e)} (1985) | MST radar | Horizontal wind speed | No theoretical explanation offered | 3×10^{-7} - 1×10^{-3} | Slope of -2 fits stratospheric (alt. 13.4 km) data in the range of frequencies 10^6 to 10^4 Hz and tropospheric (alt. 9.1 km) data in the range 10^6 to $\sim 8 \times 10^4$ Hz |
| Meek <i>et al.</i> ^{f)} (1985) | MST radar | Horizontal wind speed | The slope of the best fit line is ~ 1.5 | 4×10^{-7} - 3×10^{-4} , 5×10^{-5} - 3×10^{-3} | Reference slope of -1.5 is shown Slope of $-5/3$ fits data. |
| Gardner and Voelz ^{g)} (1987) | Lidar | Na density | $-5/3$ power law is predicted | 2×10^{-5} - 7×10^{-4} | The observed exponents are: 2.18 in summer, 1.73 in winter. |
| Kwon <i>et al.</i> ^{h)} (1990) | Radar, ground-based and airborne lidar | Wind speed, Na density | No theoretical explanation offered | 3×10^{-5} - 1×10^{-2} | Whole Na layer 1.52, top side of the layer 1.12 Bottom side -1.77 |
| Fritts <i>et al.</i> ⁱ⁾ (1990) | MU Radar | Wind speed | No theoretical explanation offered | 1×10^{-5} - 2×10^{-3} | Reference slopes of $-5/3$ and -2 are shown |
| Beatty <i>et al.</i> ^{j)} (1992) | Rayleigh/Na lidar | Passive scalar concentration | No theoretical explanation offered | 9×10^{-5} - 3×10^{-3} (range for linear regression) | Single day 1.7 Average exponent over 21 nights 1.85 ± 0.23 |
| Sica and Russell ^{k)} (1999) | Rayleigh/Na lidar | Passive scalar concentration | Claim average slope of -2 | 5×10^{-5} - 2×10^{-2} | Exponents from 1.2 to -2.7 |

a) The data used to construct the wide frequency-range power density spectrum were taken by MRI anemometer from 1500 LST on March 14 through 1200 LST on May 1, 1967 and by the AN/GMQ-12 anemometer from 1105 LST on April 10 to 1600 LST on April 18, 1967.

b) Time ranges for wind fluctuations are: at 8 km from 6 minutes to 83 days; at 86 km from 3 minutes to ~ 30 days.

c) Zonal and meridional wind measurements made with the Poker Flat MST radar over a 40-day period are used to calculate the frequency power spectra at heights between 5.99 km and 14.69 km. The finest temporal resolution is

- 1 hour. Regression is made for frequencies in the range from 0.015 h^{-1} to 0.45 h^{-1} . In some cases this range includes an obviously noisy range.
- d) The time range is from 1 minute to ~750 minutes. No linear regression is made by the authors.
- e) Horizontal wind values are formed into 4096-point data sets comprising 34 day sequences of 12-min averaged data points. No linear regression is made by the authors.
- f) 1 h to 720 h time series and 33 5 min to 6 h were used.
- g) Observed periods from 25 min to 800 min.
- h) Time series from 100 s to ~8 h are used. Temporal regressions are made over temporal scales from 30 to 360 min. Top side layer spectrum looks noisy, bottom side one fits -5/3 power law quit well.
- i) Spectra at higher altitudes look noisy, but fit -5/3 power law. Lower altitude spectra fit -2 power law well.
- j) Temporal resolution is 2 min for Na data and 5 min for Rayleigh data. Linear regression fit was performed over the frequency range from $\sim (3 \text{ h})^{-1}$ to $(5 \text{ min})^{-1}$. The authors did not separate cases close to -5/3 and -2 slopes. That is why confidence interval is rather wide (1.62 - 2.06).
- k) Strong deviation from -5/3 and -2 slopes are observed in the cases when regression includes obvious high and/or low frequency artefacts range.

3. ANALYSIS IN ORTHOGONAL DIRECTIONS: VERTICAL, TIME

3.1 Vertically pointing lidar data

In this paper, in addition to a reanalysis of the airborne data discussed in (Lilley *et al.* 2006), we also use ground-based, upward pointing lidar data from PACIFIC 2001 experimental campaign, as well as data from the MSC CARE facility. The ground based laser was operated at the fundamental wavelength of 1064 nm, suited for the detection of particles with diameter of the order of $1 \mu\text{m}$ and had a pulse repetition rate of 10 Hz (Strawbridge and Snyder 2004). The measured backscatter ratio B was averaged over various time intervals (see table 2); the result was a 2D

vertical-time planar section. All the detectors used log amplifiers – important due to the wide dynamical range of the backscatter.

Table 2 presents main characteristics of the experimental data sets. Langley0807 and Langley0808 were acquired with ground based lidar during PACIFIC 2001 in Langley, British Columbia on August 7, 8. Egbert0530 Egbert0602 Egbert0616 and Egbert0626 are from a CARE 2003 ground based lidar experiment, acquired in Egbert, Ontario on 30 May, 02, 16 and 26 June respectively. Pacific0815t8 Pacific0815t6 Pacific0815t22 Pacific0814t5 Pacific0814t7 and Pacific0814t9 are PACIFIC 2001 airborne lidar platform experiments acquired in the Lower Fraser Valley, BC on 14 and 15 August (see Lilley *et al.* 2006).

Table 2. Main parameters of experimental data sets

| Name | Type of data | Object type | Resolution* | Dimensions† |
|----------------|---------------------|--------------|---------------|-------------|
| Langley0807 | Vertical-time | aerosol | 2.997m×1.0s | 300×4990 |
| Langley0808 | Vertical-time | aerosol | 2.997m×1.0s | 300×5036 |
| Egbert0530 | Vertical-time | cirrus cloud | 3.746m×0.5s | 904×11468 |
| Egbert0602 | Vertical-time | cirrus cloud | 3.746m×30.0s | 1536×828 |
| Egbert0603 | Vertical-time | aerosol | 3.746m×30.0s | 486×648 |
| Egbert0616 | Vertical-time | cirrus cloud | 3.746m×30.0s | 800×752 |
| Pacific0815t6 | Vertical-horizontal | aerosol | 2.997m×100.0m | 372×952 |
| Pacific0815t8 | Vertical-horizontal | aerosol | 2.997m×100.0m | 844×776 |
| Pacific0815t22 | Vertical-horizontal | aerosol | 2.997m×100.0m | 956×932 |
| Pacific0814t5 | Vertical-horizontal | aerosol | 2.997m×100.0m | 384×750 |
| Pacific0814t7 | Vertical-horizontal | aerosol | 2.997m×100.0m | 386×846 |
| Pacific0814t9 | Vertical-horizontal | aerosol | 2.997m×100.0m | 372×846 |

* First number is vertical resolution in m, second is time or horizontal resolution, horizontal resolution of vertical-horizontal section data sets is estimated with airplane speed of 100 m s^{-1} .

† Vertical dimension × time or × horizontal.

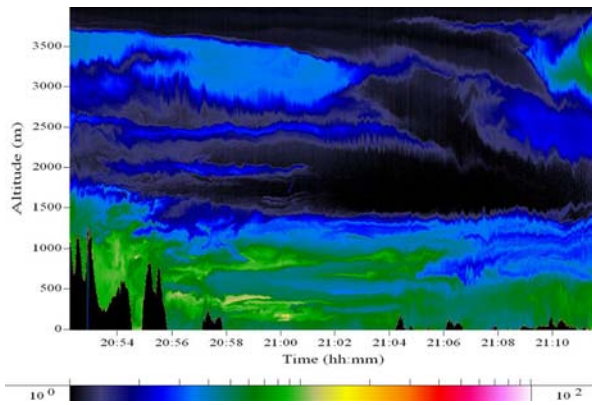


Figure 1. This is the Pacific0815t6 data taken on 15 August 2001. The scale (bottom) is logarithmic: darker is for smaller backscatter (aerosol density surrogate), lighter is for larger backscatter. In this panel, the vertical is 4.0 km and the horizontal is 120 km (log scale). The horizontal resolution is 100 m and the vertical resolution is 2.997 m. The black shapes along the bottom are mountains in the British Columbia region. There are no bad pixels in the image. There is no saturated signal and there is high sensitivity to low signal return.

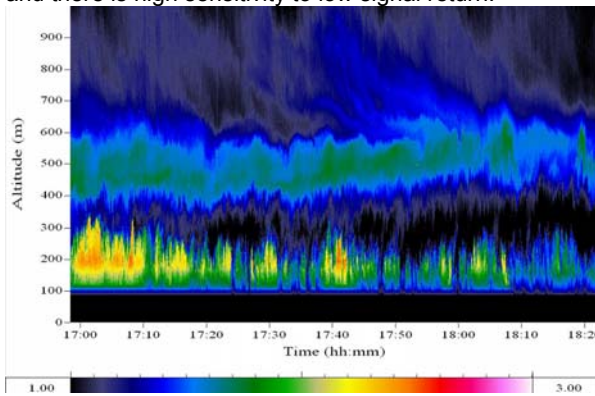


Figure 2. This is the Langley0808 data taken on 8 August 2001. The scale (bottom) is linear: darker is for smaller backscatter (aerosol density surrogate), lighter is for larger backscatter. In this panel, the vertical is 1.0 km and the time is 5000 s (due to the signal weakness, the scale is linear). The time resolution is 1.0 s and the vertical resolution is 2.997 m. There are no bad pixels in the image. There is no saturated signal and there is high sensitivity to low signal return.

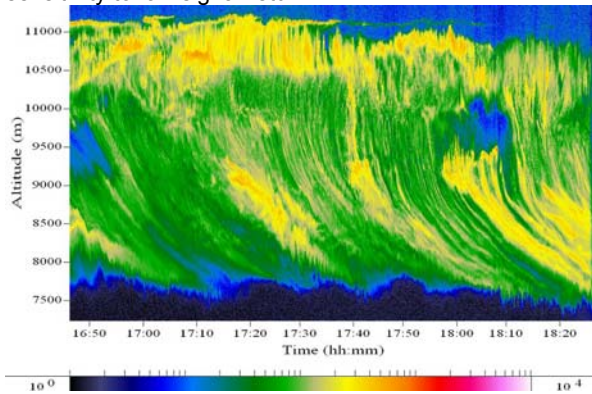


Figure 3. This is the Egbert0530 data taken on 30 May 2003. The scale (bottom) is logarithmic: darker is for smaller backscatter (cirrus density surrogate), lighter is for larger backscatter. In this panel, the vertical is 4.3 km and the time is 5900 s (log scale). The time resolution is 0.5 s and the vertical resolution is 3.746 m. There is no saturated signal and there is high sensitivity to low signal return.

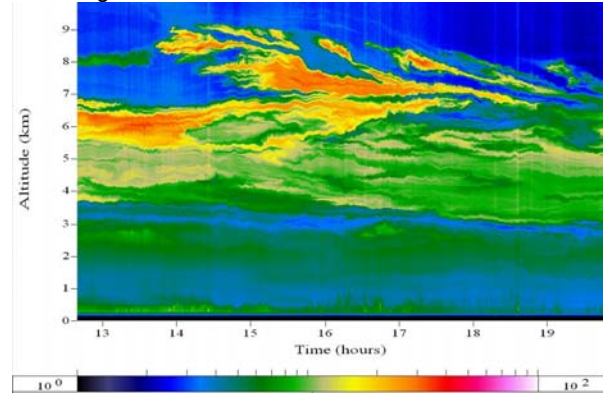


Figure 4. This is the Egbert0602 data taken on 2 June 2003. The scale (bottom) is logarithmic: darker is for smaller backscatter (cirrus density surrogate), lighter is for larger backscatter. In this panel, the vertical is 4.3 km and the time is 5900 s (log scale). The time resolution is 30.0 s and the vertical resolution is 3.746 m. There is no saturated signal and there is high sensitivity to low signal return.

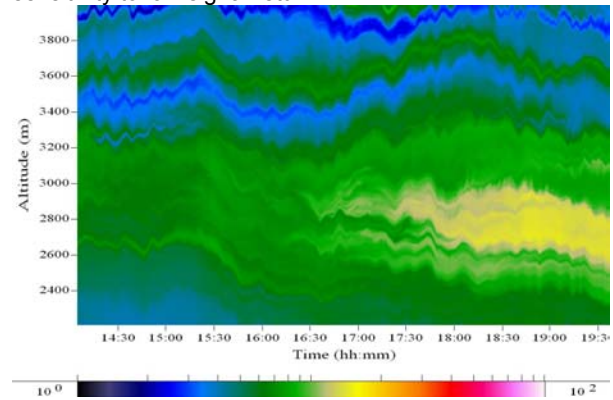


Figure 5. This is the Egbert0603 data taken on 3 June 2003. The scale (bottom) is logarithmic: darker is for smaller backscatter (aerosol density surrogate), lighter is for larger backscatter. In this panel, the vertical is 1.82 km and the horizontal is 19440 s (log scale). The time resolution is 30.0 s and the vertical resolution is 3.746 m. There is no saturated signal and there is high sensitivity to low signal return.

3.2 The space-time scaling for passive scalars

We have seen in part I, II and in the introduction how the classical Kolmogorov law can be extended to anisotropic space-time taking into account the buoyancy forces in the vertical. The key part of the model is the replacement of the

usual Euclidean distance by a scale function. Lilley *et al.* (2004) showed how this could be used to obtain an anisotropic extension of the classical Corrsin-Obukhov law for passive scalar diffusion. Extending this to space-time, we have

$$\llbracket (\Delta \mathbf{r}, \Delta t) \rrbracket = \Theta(\Omega') \llbracket (\Delta \mathbf{r}, \Delta t) \rrbracket_{can} \quad (4)$$

where Ω' defines direction in the nonlinearly transformed space $(\Delta \mathbf{r}', \Delta t')$ (see below) so that $\Theta(\Omega')$ represents the shape of unit ball, $\llbracket \Delta \mathbf{r}, \Delta t \rrbracket_{can}$ is the canonical scale function; see (1c). An anisotropic scaling generalization of the Corrsin-Obukhov law for fluctuations in passive scalar concentration is obtained by replacing the usual distance function by a scale function:

$$\Delta \rho(\Delta \mathbf{r}, \Delta t) = \chi^{1/2} \varepsilon^{-1/6} \llbracket \Delta \mathbf{r}, \Delta t \rrbracket^{1/3} \quad (5)$$

where χ is the passive scalar variance flux. In orthogonal directions, the above implies the same scaling as for the horizontal velocity discussed earlier, including the same limiting cases in time according to the magnitude of the advection velocity.

3.3 Analysis in the vertical

Before turning to a more complete analysis of the data we can already check equations (4), (5) above by considering the 1D spectra only in time or only in the vertical. The results are given with Fig. 6. We can clearly see the Bolgiano-Obukhov (BO) scaling in the vertical. Some deviations from the theoretically predicted slope are due to problems with lidar attenuation corrections (see especially the second spectrum from the top in Fig. 6). This means that values the backscatter ratio are too smooth over the highest factor of 8 or so in scale. This problem arises due to the inadequate dynamical range of the digitizer so that – to within one digital count – successive raw values are nominally the same, i.e. spuriously smoothed (see Gagnon *et al.* (2006) for a quantitative analysis of this effect). In this case (Egbert0602) we avoided the problem by degrading the vertical resolution by a factor of 8 before proceeding to the refined analyses discussed below. As far as we can tell, the cirrus and aerosol scalings are the same and both are compatible with the anisotropic extension of the Corrsin-Obukhov law. We can see that BO $\beta_v = 11/5$ works well in wide (up to 2 orders) range of scale.

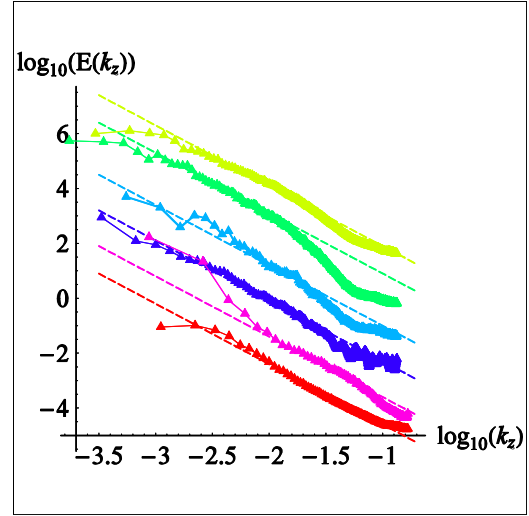


Figure 6. 1D space (vertical) energy spectra as function of vertical wave number k (in m^{-1}) for vertical-time data sets: yellow – Egbert0530 (cirrus cloud), green – Egbert0602 (cirrus), blue – Egbert0603 (aerosol), dark blue – Egbert0616 (aerosol), pink – Langley0807 (aerosol), red – Langley0808 (aerosol). Dashed lines are reference theoretical slopes of $-11/5$

3.4 Analysis in time

Ignoring the y coordinate (equivalently, orienting our system so that the x axis is parallel to the horizontal component of the wind), applying (5) with the (advected) scale function 1b, we obtain:

$$\Delta \rho(\Delta x, \Delta z, \Delta t) = \chi^{1/2} \varepsilon^{-1/6} l_s^{1/3} \times \left[\left(\frac{\Delta x - v_x \Delta t}{l_s} \right)^2 + \left(\frac{\Delta z - v_z \Delta t}{l_s} \right)^{2/H_z} + \left(\frac{\Delta t}{\tau_s} \right)^{2/H_t} \right]^{1/6} \quad (7)$$

Putting $\Delta x = \Delta y = 0$, we can now see that the pure time behaviour has three terms which dominate depending on the parameters as analyzed in section 2(a), i.e. the same three regimes as for the velocity field: $\beta_\tau = 5/3, 11/5, 2$ (domination by the horizontal and vertical wind terms and the pure time development term, the vertical wind term respectively).

To determine the temporal behaviour for vertical-time data sets we made standard 1D Fourier power spectrum analysis in time. The results are represented by Fig. 7; we see that there are three cases with $\beta_\tau = 2$ are Egbert0602 (green line) and Egbert0603 (blue line), and three other cases show $\beta_\tau = 5/3$.

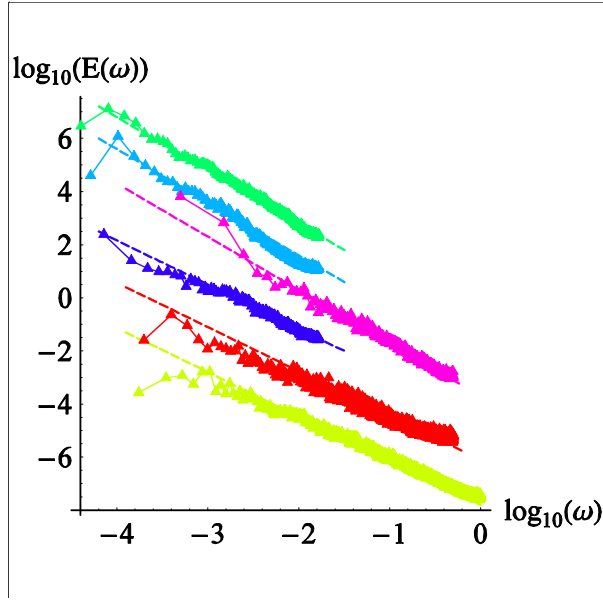


Figure 7. 1D temporal energy spectra as a functions of frequency ω (in s^{-1}) for vertical-time data sets: yellow – Egbert0530 (cirrus cloud), green - Egbert0602 (cirrus), blue - Egbert0603 (aerosol), dark blue - Egbert0616 (aerosol), pink – Langley0807 (aerosol), red - Langley0808 (aerosol). Dashed lines are reference theoretical slopes of -2 (green and blue) and -5/3 (all other).

4. ARBITRARY DIRECTIONS IN SPACE-TIME

4.1 The ASAT technique

In section 3(c), 3(d), we analysed the data in orthogonal directions (vertical, time); this is only a partial analysis it does not allow us to test the theory at intermediate angles, nor estimate the function characterizing the “trivial anisotropy” $\Theta(\Omega)$. We now describe a new “Anisotropic Scaling Analysis Technique” (ASAT) method for doing this. First, taking advantage of the fact that the observed temporal behaviour was pure power law the (z,t) plane, fluctuations can be written:

$$\Delta\rho(\Delta z, \Delta t) = \Delta\rho(0, 0, \Delta z, \Delta t) = \chi^{1/2} \phi^{-1/4} \varepsilon^{1/4} \Theta^{1/3}(\theta) \left[\left(\frac{\Delta z}{l_s} \right)^{2/H_z} + \left(\frac{\Delta t}{\tau_s} \right)^{2/H_t} \right]^{1/6} \quad (8a)$$

with $H'_t=1$ for horizontal wind domination and $H'_t=H_t=2/3$ for pure temporal development. The (x,z) plane fluctuations can be written in the analogous way:

$$\Delta\rho(\Delta x, \Delta z) = \Delta\rho(\Delta x, 0, \Delta z, 0) = \chi^{1/2} \phi^{-1/4} \varepsilon^{1/4} \Theta^{1/3}(\theta') \left[\left(\frac{\Delta x}{l_s} \right)^2 + \left(\frac{\Delta z}{l_s} \right)^{2/H_z} \right]^{1/6} \quad (8b)$$

where Θ is function only of the polar angle θ' in the nonlinearly transformed space described in eq. (9) below.

Assuming that the orthogonal (z and t) analyses have determined the exponents H_z , H_t , we can now remove the nonlinear (differential) space-time stratification so as to determine the remaining “trivial” anisotropy characterized by $\Theta(\Omega)$. To do this, it suffices to make the following nonlinear transformation of variables:

$$z' = \left| \frac{\Delta z}{\Delta z_{ref}} \right|^{1/H_z} \text{sign}(\Delta z), \quad t' = \left| \frac{\Delta t}{\Delta t_{ref}} \right|^{1/H_t} \text{sign}(\Delta t) \quad (9a)$$

or

$$z' = \left| \frac{\Delta z}{\Delta z_{ref}} \right|^{1/H_z} \text{sign}(\Delta z), \quad x' = \frac{\Delta x}{\Delta x_{ref}} \quad (9b)$$

where Δz_{ref} , Δt_{ref} are convenient reference distances and times respectively (taken here so that distances and times can be given in dimensionless spatial and temporal “pixels”; the shape function $\Theta(\theta')$ will depend on this choice). In this nonlinear (“primed”) space, we have the following polar coordinates:

$$R' = [z'^2 + t'^2]^{1/2}, \quad \theta' = \arctan[z'/t'] \quad (9c)$$

so:

$$\Delta\rho(R', \theta') \sim \Theta^{1/3}(\theta') R'^{1/3} \quad (9d)$$

where $\Theta(\theta')$ represents the shape of all the balls in the (z', t') space. The virtue of this nonlinear transformation is that in (z', t') space, the scaling is symmetric under isotropic scale transformations, i.e. with $G =$ the identity so that more traditional isotropic analysis methods can be used. $\Theta(\theta')$ thus determines the remaining “trivial” anisotropy in the (z', t') space; it also determines the unit ball in (z, t) space. Equations (9) are the basis of the ASAT. It allows us to simultaneously verify the anisotropic scaling hypothesis (8) in arbitrary non-

orthogonal directions while determining the function $\Theta(\theta')$ in the space $(\Delta z', \Delta t')$. In the next sections we discuss how to use structure functions and spectra to estimate Θ , and in section 4.4 we discuss the interpretation of the result. For further analysis it is convenient to introduce another form of scale function in 2D (z, t) domain:

$$\begin{aligned} \left[\left[(\Delta z, \Delta t) \right] \right]^* &= l_s \Theta^*(\theta') \left[\left(\frac{\Delta t}{\tau_s} \right)^2 + \left(\frac{\Delta z}{l_s} \right)^{2/h} \right]^{1/2}; \quad (10a) \\ h &= H_z / H_t' \end{aligned}$$

which satisfies the basic scaling equation with generator $G^* = G / H_z$. This scale function is connected with the scale function used in (8a) with the following relationship:

$$\left[\left[(\Delta z, \Delta t) \right] \right]_{G^*} = \left[\left[(\Delta z, \Delta t) \right] \right]_G^{1/H_z} \quad (10b)$$

This allows us to rewrite (8a) in the following form

$$\begin{aligned} \Delta \rho(\Delta z, \Delta t) &= \chi^{1/2} \phi^{-1/4} \varepsilon^{1/4} \Theta^{*1/3}(\theta') \times \\ &\left[\left(\frac{\Delta t}{\tau_s} \right)^2 + \left(\frac{\Delta z}{l_s} \right)^{2/h} \right]^{1/(6H_z)} \quad (10c) \end{aligned}$$

Finally we can analyze (x, z) cross-sections playing with only one parameter $h = H_z$ in the way unified with analysis of (x, z) cross-sections:

$$\begin{aligned} \left[\left[(\Delta x, \Delta z) \right] \right]^* &= l_s \Theta^*(\theta') \left[\left(\frac{\Delta x}{l_s} \right)^2 + \left(\frac{\Delta z}{l_s} \right)^{2/h} \right]^{1/2}; \quad (10d) \\ h &= H_z \end{aligned}$$

4.2 The ASAT technique in real space: anisotropic structure functions

To verify (8) we consider the 2D Structure Function (SF) dependence on primed radial polar coordinate R' for fixed value of angle Ω' in the space $(\Delta z', \Delta t')$. We use the following definition

$$\begin{aligned} \Delta \rho &= |\rho(z + \Delta z, t + \Delta t) - \rho(z, t)| \\ S_q(R', \theta') &= \left\langle |\Delta \rho|^q \right\rangle \quad (11a) \end{aligned}$$

From (5) taking q^{th} powers and ensemble averaging, we see that:

$$\begin{aligned} S_q(R', \theta') &= \left\langle \chi_{R'}^{q/2} \varepsilon_{R'}^{-q/6} \right\rangle \Theta(\theta')^{q/3} R'^{q/3} = \\ &(\Theta(\theta') R')^{\xi(q)} \quad (11b) \end{aligned}$$

Recall that the random fluxes $\chi_{R'}$, $\varepsilon_{R'}$ are defined as averages at the scale R' thus have a scale dependence responsible for the “intermittency corrections” (i.e. the nonlinear part of the structure function exponent $\xi(q)$, see section 4(e) below). However, taking $q=1$ these corrections will be small, $\xi(q) \approx Hq = H=1/3$. Testing this on the data, we obtain Figs. 8(a), 9(a), 10(a) and 11(a). As one can see by the parallel lines for various θ' 's, the theory works well over a wide range of scales for both cirrus clouds and aerosols', for both advection free and advection dominant cases of temporal development. The difference between the 1D structure functions in different directions means that the unit ball is not a circle (sphere). To clearly see this “trivial” anisotropy we calculated the “compensated” 2D SF averaged over $\log_{10}(R')$:

$S_{c,1} = \left\langle R'^{-1/3} S_1(R', \theta') \right\rangle_{\log R'} \approx \Theta(\theta')^{1/3}$ as function of polar angle θ' - it represents the shape of the unit ball. $S_{c,1}$ is useful because - within rather small intermittency corrections - it is expected to be independent of R' . Figures 8(b), 9(b), 10(b), and 11(b) were determined from tables of $R'^{-1/3} S_1$ values as functions of $\log_{10}(R')$ and θ' with increments of $\log_{10}(R') = 0.2$. Along rays of fixed angle Ω' , the relative error (the ratio of $S_{c,1}$ and standard deviation) does not exceed 10% over wide ranges of scale ($R'_{\text{max}} / R'_{\text{min}} > 10^3$ in many instances); often this variation does not exceed 5% (see Fig. 11(b)). The ranges chosen for averaging are indicated in the captions for the figures. Thus, new ASAT technique applied to first order ($q=1$) 2D structure function analysis allows us to verify the theory to within about 10% over more than 3 orders of magnitude of space-time or space-space scales. On the other hand it provides more convincing verification of the theory since it permits analysis in non-orthogonal directions. Note that from its definition, the structure functions are symmetric with respect to inversion about the origin; see appendix A.

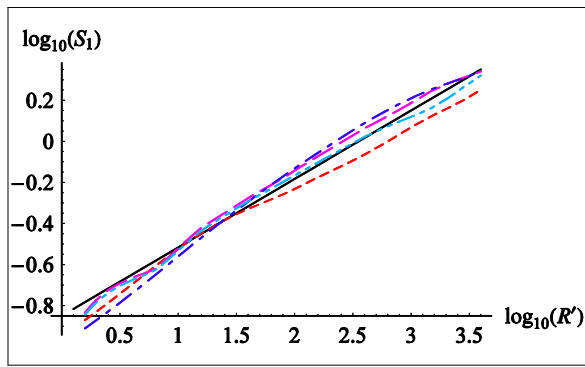


Figure 8(a). 2D Structure function S_1 as function of R' for 4 directions ($\theta' = 0$ (red, short dashes), $\pi/4$ (magenta long dashes), $\pi/2$ (blue, long, short dashes), $3\pi/4$ (light blue long, short, short dashes) in nonlinearly transformed space for Egbert0603. Black line – theoretical slope of $1/3$.

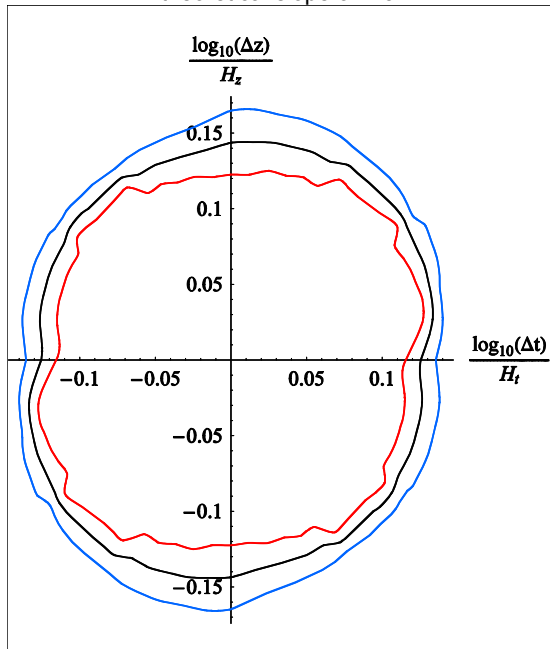


Figure 8(b). Compensated structure function $R'^{-1/3} S_1(\log_{10}(R'), \theta')$ averaged over $0.2 < \log_{10}(R') < 3.4$ for Egbert0603 (black line). Red and blue lines are compensated averaged 2D SF plus/minus standard deviation.

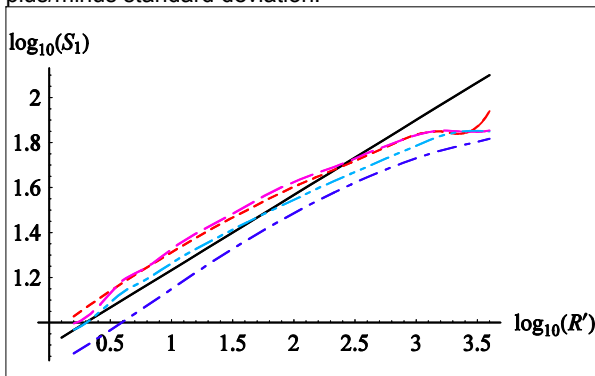


Figure 9(a). Same as 8(a) but for Egbert0530.

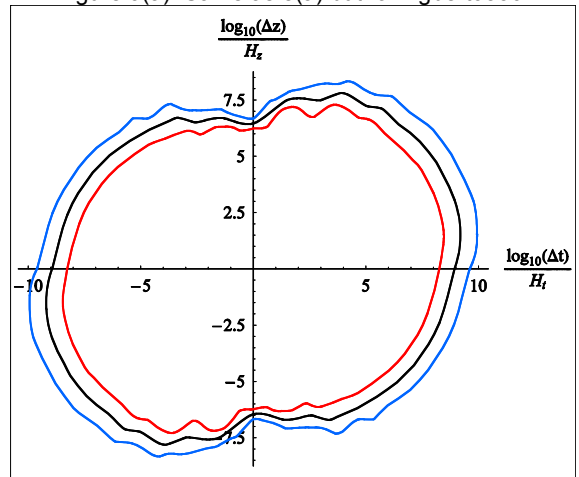


Figure 9(b). Same as 8(b) but for Egbert0530, averaging over $0.2 < \log_{10}(R') < 2.6$.

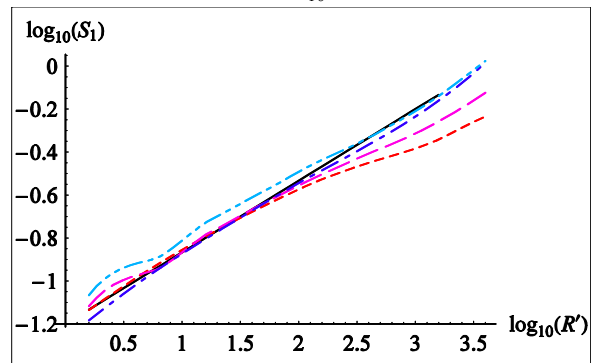


Figure 10(a). Same as 8(a) but for Langley0807.

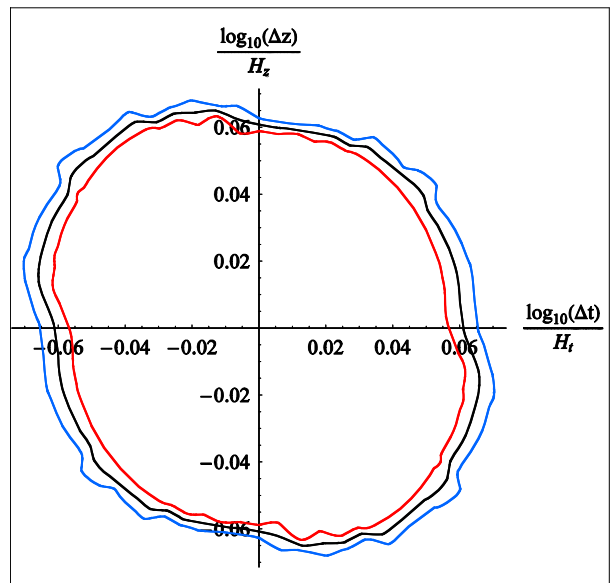


Figure 10(b). Same as 9(b) but for Langley0807, averaging over $0.2 < \log_{10}(R') < 2.4$.

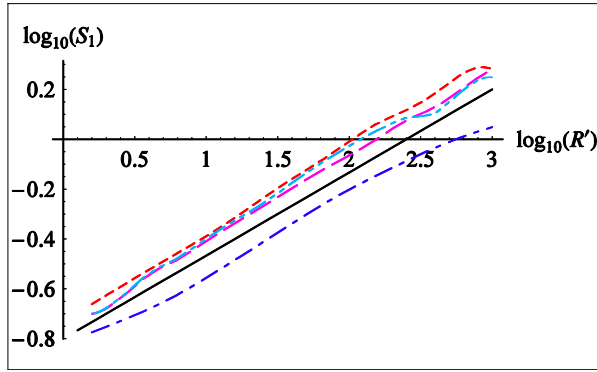


Figure 11(a). Same as 8(a) but for Pacific0815t6.

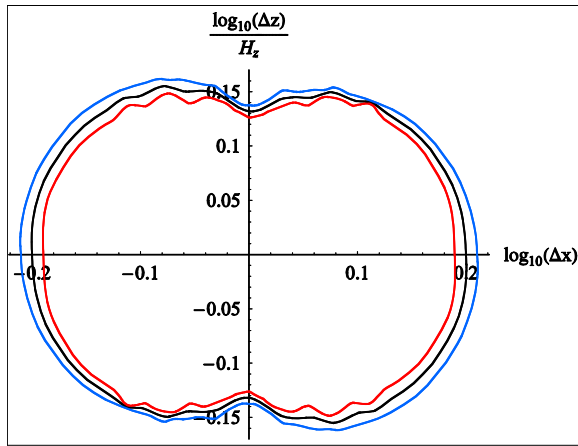
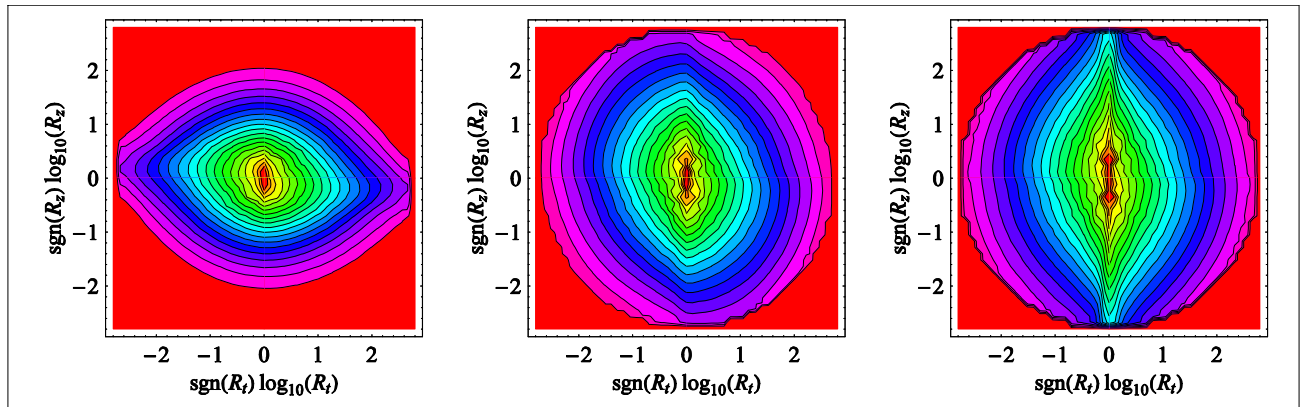


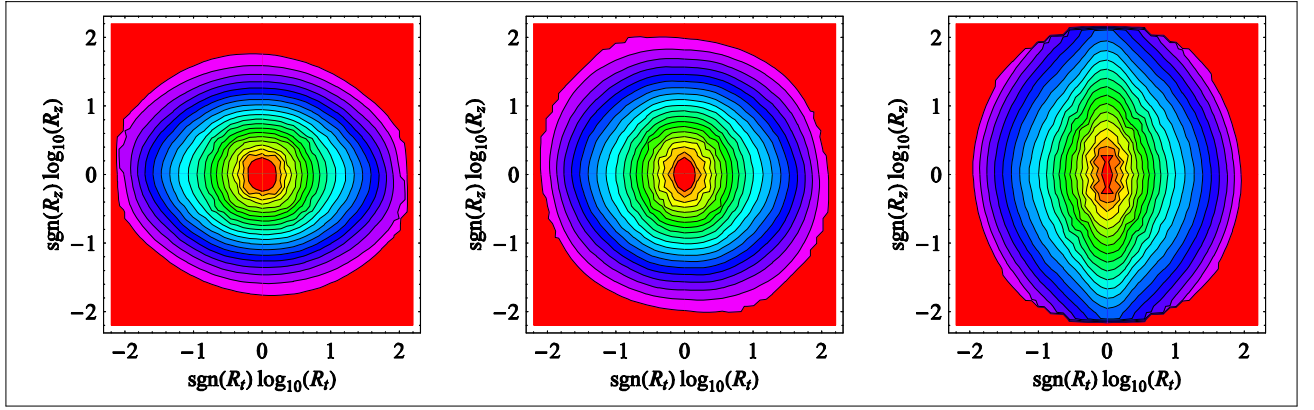
Figure 11(b). Same as 8(b) but for Pacific0815t6, averaging over $0.2 < \log_{10}(R') < 2.8$.

Figures 12(a), (b) and (c) show a comparison of contour plots of $\log(S_1(\log(R'/R_i), \theta'))$ with nonlinear transformation (9a) corresponding to

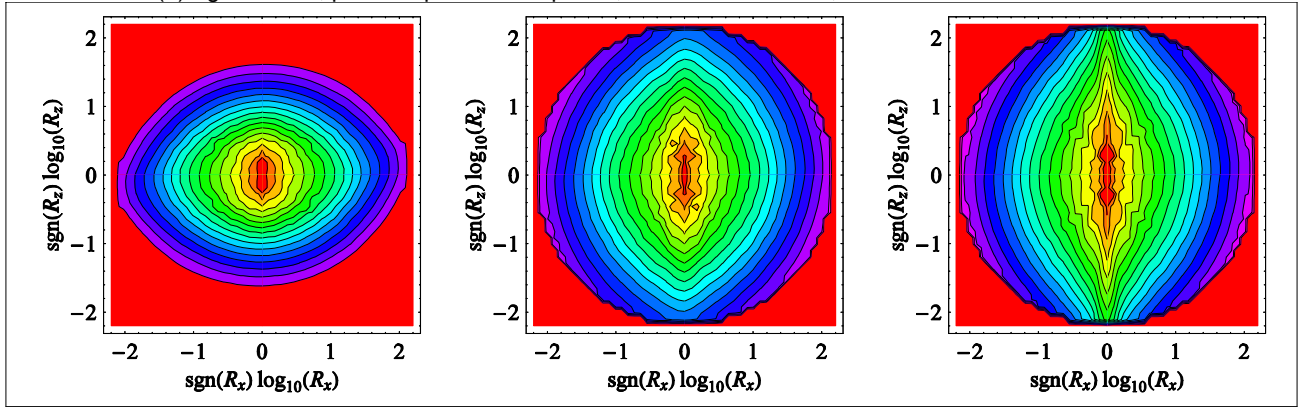


(a) Egbert 0530, wind domination; the vertical axis is z , the horizontal axis is t

different theories: isotropic turbulence, 29/9D model and gravity waves. If the contours of $\log(S(R', \theta'))$ are invariant under an isotropic scale change (they have the same shapes), then the corresponding contours of $\log(S_1(\log(R'/R_i), \theta'))$ do not have the same shapes but are rather equally spaced in all directions (R_i is a nondimensionalizing inner scale; below R_i , the signal is dominated by instrumental noise). The advantage of using a $(\log(R'/R_i), \theta')$ space representation is that we can visually represent a much wider range of scales on the same picture. The analysis is done using the alternative scale function (10a). For the left column corresponding to $h = H_z / H'_i = 1$, i.e. no transformation of coordinates, we can see that as we move from contour to contour, the spacing between the contours is different in the horizontal and vertical directions. For the middle case (using the theoretical transformation from the 29/9 model), we can see that the contours are spaced pretty much the same distance apart (i.e. equally spaced in all directions as expected). Finally in the right hand column, the gravity wave value of $h = H_z / H'_i$ is used in the transformation, again leading to contours which are not equally spaced – this time they are closer in the vertical than in the horizontal. Note that all the contours are spaced at equal factors of S_1 of 1.12 (for the 29/9 model i.e. with $H=1/3$, this corresponds to a factor of 1.41 in scale), the total range of scales is roughly 100.



(b) Egbert 0603, pure temporal development; the vertical axis is z , the horizontal axis is t



(c) Pacific 2001 0815t6, vertical – horizontal cross-section; the vertical axis is z , the horizontal axis is x
 Figure 12. Contour plot of S_1 with different nonlinear transformation: left - Isotropic turbulence (no transformation, $h = 1$); center - 29/9 model: (a) $h = H_z / H'_t = 5/9$, (b) $h = H_z / H'_t = 5/6$, (c) $h = H_z = 5/9$ (see (10c) for cases (a) and (b) and (10d)); right - gravity waves: (a) $h = 1/3$, (b) $h = 1/2$, (c) $h = 1/3$.

4.3 ASAT in Fourier space: analysis of (z,t) and (x,z) cross-sections

ASAT can also be applied in Fourier space to spectral densities of η powers of the original field. For $\eta=1$, we obtain essentially the Fourier transform of S_2 (the Wiener-Khinchin theorem). Although there is no fundamental difference, in Fourier space, the scales are better separated (so that if scale breaks are present they are sharper, better defined) and due to the FFT algorithm, it is more convenient to estimate than S_1 . In addition, S_1 will only converge to nontrivial results for $0 < H < 1$ (the case here) whereas the spectra have no corresponding restriction. Again, we consider 2D z,t cross-sections. The power spectral density has the following scaling

$$P(k_z, \omega) = \langle |\tilde{\rho}(k_z, \omega)|^2 \rangle \sim \|\mathbf{k}\|^{-s} \quad (12)$$

where $\tilde{\rho}(k_z, \omega)$ is the Fourier transform of $\rho(z, t)$ scale function $\|\mathbf{k}\|$ has the following form:

$$\|\mathbf{k}\| = \tilde{\Theta} \|\mathbf{k}\|_{can}; \quad (13)$$

$$\|\mathbf{k}\|_{can} = l_s^{-1} \left((k_z l_s)^{2/H_z} + (\tau_s \omega^{2/H_t}) \right)^{1/2}$$

1D analysis in time and vertical directions based on the relation between the 1D and 2D spectra:

$$\int_{-\infty}^{+\infty} P(k_z, \omega) dk_z = E(\omega) \propto \omega^{-\beta_t},$$

$$\int_{-\infty}^{+\infty} P(k_z, \omega) d\omega = E(k_z) \propto k_z^{-\beta_v}$$

This allows us to obtain the exponent s in terms of the 1D spectral exponents:

$$\int_0^{\infty} (k_z^{2/H_z} + \omega^{2/H_t})^{-s/2} d\omega \sim k_z^{H_t/H_z(-s/H_t+1)}; \quad s > H_t, \quad k_z > 0$$

$$\int_0^{\infty} (k_z^{2/H_z} + \omega^{2/H_t})^{-s/2} dk_z \sim \omega^{H_z/H_t(-s/H_z+1)}; \quad s > H_z, \quad \omega > 0$$

(we are only interested in the scaling of the spectra; hence for example in the left hand integral, use the substitution $k_z = k'_z \omega$ etc.). Comparing with the definitions of the β 's, we obtain:

$$\beta_v = H_t / H_z (s / H_t - 1),$$

$$\beta_\tau = H_z / H_t (s / H_z - 1). \quad \text{Solving for } s, \text{ we obtain:}$$

$$s = \beta_v H_z + H_t = \beta_\tau H_t + H_z \quad (14)$$

which leads to the useful relation: $(\beta_v - 1) / (\beta_\tau - 1) = H_t / H_z$. Using the values; $\beta_\tau = 2$, $H'_t = 2/3$ in the case of pure temporal development, we obtain $s=17/9$ and using $\beta_\tau = 5/3$ and $H'_t = 1$ in the case of horizontal wind domination we obtain $s = \beta_\tau H_t + H_z = 20/9$.

Following the ASAT idea, we make the following nonlinear transformation of variables

$$\omega \tau_s = (k_R \cos \tilde{\theta}')^{H'_t}, \quad k_z l_s = (k_R \sin \tilde{\theta}')^{H_z}, \quad (15)$$

$$\omega' = (\omega \tau_s)^{1/H'_t}, \quad k'_z = (k_z l_s)^{1/H_z} \quad (16)$$

gives us in the space (ω', k'_z) ($(k'_R, \tilde{\theta}')$ are the polar coordinates in this space):

$$P(k'_R, \tilde{\theta}') \sim (\tilde{\Theta}(\tilde{\Omega}') k'_R)^{-s} = \tilde{\Theta}^{-s} (\tilde{\Omega}') k'^{-s}_R \quad (17)$$

Similarly, we can use the same method to re-analyze the (x, z) cross-sections discussed in (Lilley *et al.* 2006) by substitution $k_x l_s$ instead of $(k_z l_s)^{1/H_z}$ and $(k_x l_s)^{1/H_x}$ instead of $(\omega \tau_s)^{1/H'_t}$ in formulas (13), (15) and (16).

Thus, the factorization property (17) implies that contour plots of $P(k'_z, \omega')$ should give contours of the same shape at any scale (the shape only depends on the polar angle). Convincing evidence of this fact is provided by Figs. 13(a), (b) and (c). They represent 1D dependences of 2D spectrum $P(k'_R, \tilde{\Omega}')$ on k'_R along different rays $\tilde{\Omega}'$ in the space (16), they also show the corresponding spectra compensated by the theoretical behavior $(k'_R)^{-17/9}$, i.e. ignoring the small intermittency corrections). We can see clear that for all directions in the (z', t') space, the scaling

obeys (17) quite well. In this section we presented qualitative evidence that (17) is valid. Quantitative estimation of the elliptical dimensions of space-time atmospheric motions using the ASAT technique is considered in (Radkevich *et al.* 2006).

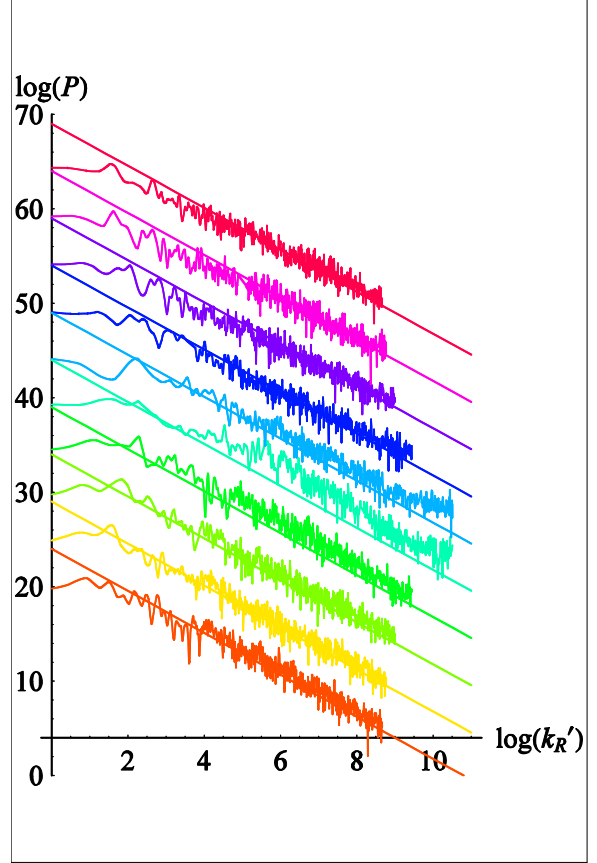


Figure 13(a). 1D dependences of spectrum $P(k'_R, \tilde{\theta}')$ for Egbert 0530 (horizontal wind domination, cirrus cloud) on k'_R along different rays $\tilde{\theta}' = \arctan(k'_z / \omega') = 0.05\pi, 0.15\pi, \dots, 0.95\pi$. Dependences for different directions are each shifted by 5 orders of magnitude. Bottom lines correspond to low values of $\tilde{\theta}'$; straight lines are reference slopes of $20/9$.

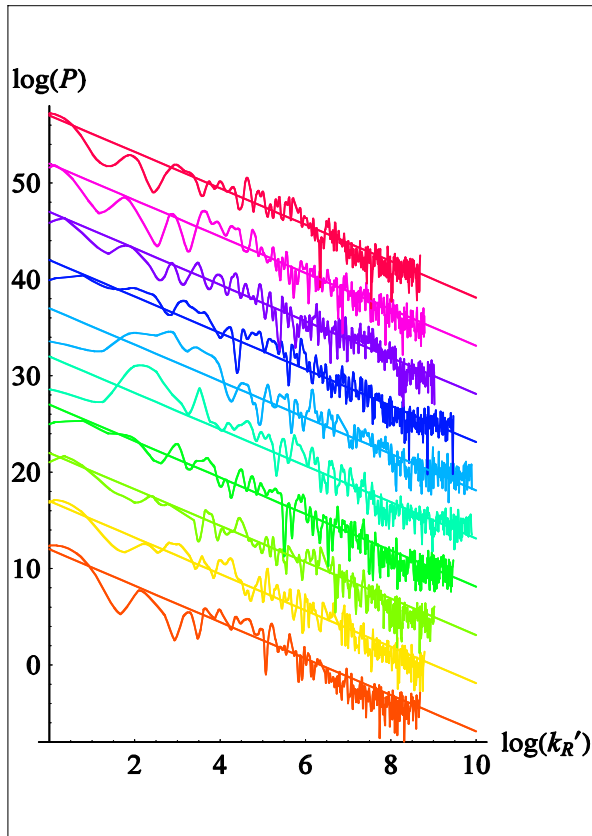


Figure 13(b). Same as 13(a) but for Egbert 0603 (pure temporal development, aerosol layers; reference slope $s=17/9$).

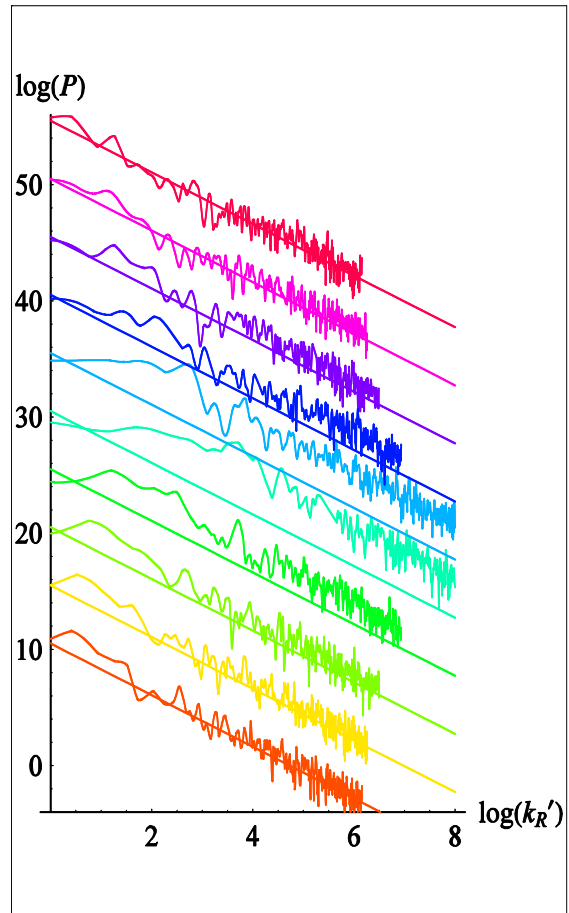


Figure 13(c). Same as 13(a) but for Pacific 2001 0815t22 (vertical-horizontal cross-section, aerosol layers, reference slope $s=20/9$).

Figures 14 give another evidence of nonlinear transformation (16). This transformation implies that contour plots of $P(k'_z, \omega')$ (or for vertical cross-sections, $P(k'_x, k'_z)$) should give contours of the same shape at any scale (it only depends on the polar angle). We can clearly see that the large and small contours after transformation (but not before) have the same shape (only depend on polar angle).

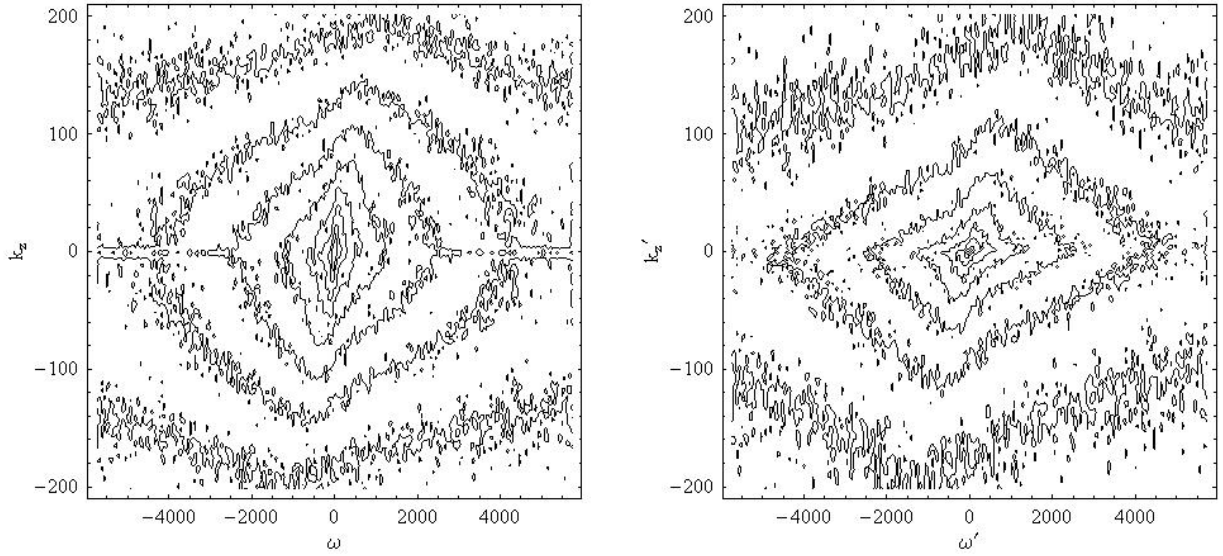


Figure 14(a). Contour plot of $\log(P(k_z, \omega))$ (left picture, before nonlinear transformation) and $\log(P(k'_z, \omega'))$ (after transformation) for Egbert 0530 data set (the case of horizontal wind “domination”). The spectra are smoothed with a radius 4 gaussian smoother in Fourier space.

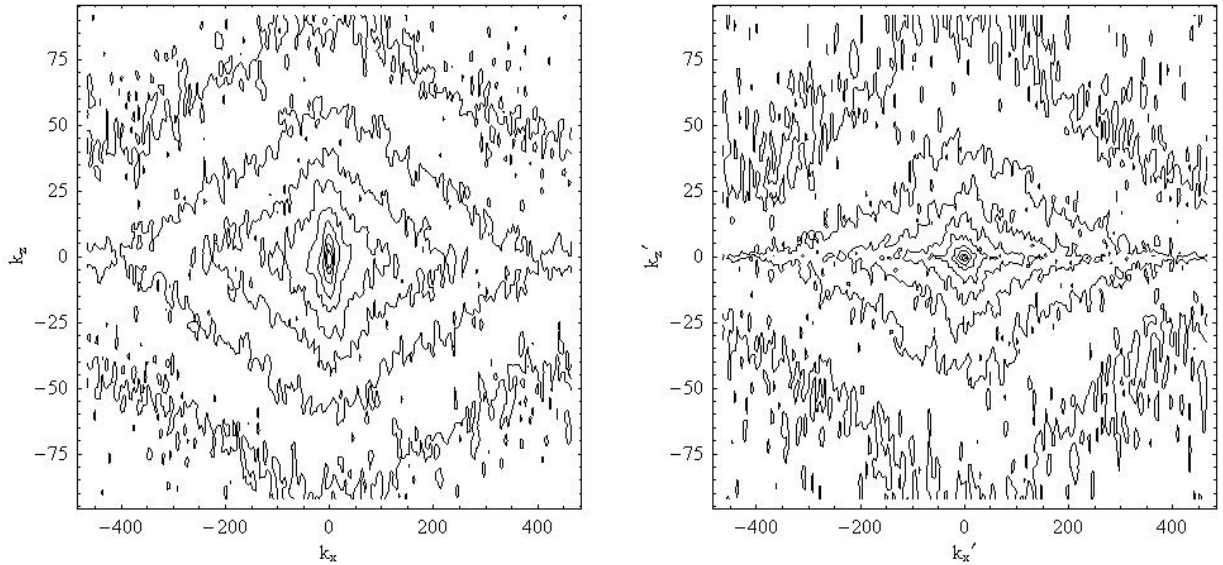


Fig. 14(b). Same as 2a but for Pacific 2001 0815t22 data set ((x,z) cross section). The spectra are smoothed with a radius 4 gaussian smoother in Fourier space.

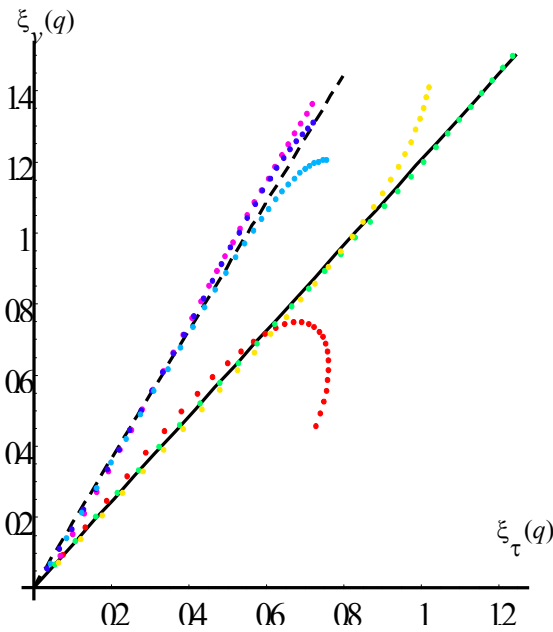
4.4 Multifractal analysis in space-time

Up until now, we have used the ASAT technique to confirm the anisotropic space-time scaling extensions of the Corrsin-Obukhov law; we did not use it to empirically estimate the theoretical exponents; in (Radkevich *et al.* 2006), we show one way of doing this. Here, we return to the method of (Lilley *et al.* 2004) (orthogonal

directions) but consider the anisotropy of the moments of all orders (i.e. including the effects of intermittency; all results discussed above are obtained for first or second order statistics S_1 , E respectively).

The q^{th} order structure function exponent $\xi(q)$ is defined in (11b). Assuming the scale functions 10 (c), 10(d), we see that for all q , the ratios of $\xi(q)$ along different coordinate axes will yield h .

Estimating $\xi(q)$ at intervals of 0.1 from $q=0.1$ to 3 we find for the 3 cases with horizontal wind domination with average $\xi_\tau/\xi_\nu = 0.54 \pm 0.02$ (theory predicts 5/9); for the cases of pure temporal behaviour $\xi_\tau/\xi_\nu = 0.81 \pm 0.04$; whereas the theory predicts 5/6. Estimated errors are standard deviations from the mean values of the ratios. These results are presented as a parametric plot of ξ_ν vs. ξ_τ in Fig. 15 (analogous to Fig. 9 in (Lilley *et al.* 2005)). Deviations from linear behaviour occur at high values of q due to



poor statistics.

Figure 15. Parametric dependence of $\xi_\tau(q)$ vs. $\xi_\nu(q)$ ($q = 0.1, 0.2, \dots, 3$) for three cases of horizontal wind domination and three cases of pure temporal development, the slopes of reference theoretical lines are $H_z/H_z=9/5$ (dashed) and $H_z/H_z=6/5$ (solid); red - Langley0807, magenta - Langley0808, blue - Egbert 0530, light blue - Egbert 0616, green - Egbert 0602, yellow - Egbert 0603. Strong deviation from theoretical behavior for some cases are due to pure statistics for high orders q .

In order to find the temporal exponent H_t we must make an assumption for H_z . Assuming the theoretical value $H_z=5/9$, we obtain

$H_t = H_z \xi_\nu(q) / \xi_\tau(q) \approx 0.68 \pm 0.03$, compared to the theoretical value $H_t=2/3$. Alternatively, assuming that H_z is structure function exponents ratio for the wind domination case $\xi_\tau/\xi_\nu = 0.54 \pm 0.02$, we obtain $H_t = (0.54 \pm 0.02) / (0.81 \pm 0.04) = 0.67 \pm 0.06$. Finally we obtain the elliptical dimension of space-time atmospheric motions which is the trace of the generator G_{st} :

$$D_{st} = Tr(G_{st}) = 2 + H_z + H_t = 29/9 \approx 3.22... \quad (19)$$

The experimental values based on theoretical and empirical H_z are $D_{st} \approx 3.24 \pm 0.03$ and $D_{st} \approx 3.21 \pm 0.06$ respectively, which is again very close to the theoretical prediction (19).

Now, taking into account convincing evidence of stratification exponents, we can estimate sphero-scale l_s . In order to do this we plotted a horizontal-vertical analogue of the space-time Stommel diagrams which establish relationships between displacements in orthogonal directions corresponding to the same fluctuation of density. Using theoretical extrapolation of the diagrams we found intersections with bisector which take place at sphero-scales. The results are given with Table 3. We see that values of l_s are distributed from 14 cm to 2.34 m.

Table 3. Estimations of sphero-scale

| Data set | l_s , m |
|----------|-----------|
| 0814t5 | 0.58 |
| 0814t7 | 0.36 |
| 0814t9 | 0.39 |
| 0814t17 | 0.77 |
| 0814t20 | 0.94 |
| 0815t6 | 0.14 |
| 0815t8 | 0.36 |
| 0815t10 | 0.34 |
| 0815t18 | 2.34 |
| 0815t22 | 0.27 |

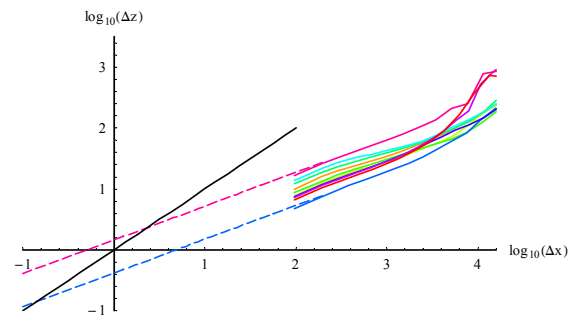


Figure 16. Horizontal vertical scale diagrams for different vertical horizontal data sets. Dashed pink and

blue lines are theoretical extrapolation for the highest and lowest diagrams. Black line – bisector.

Vertical-time Stommel diagrams are presented in fig. 17. They give qualitative evidence of vertical and temporal stratification exponents.

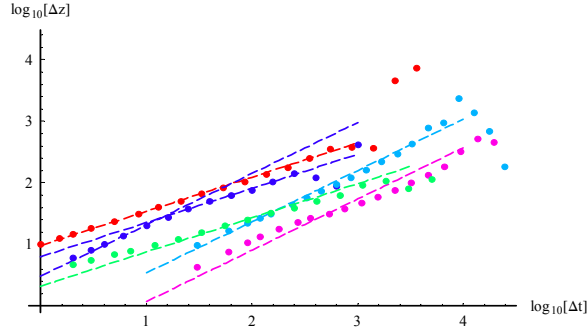


Figure 17. Vertical-time Stommel diagrams for different vertical-time data sets. Dashed lines are theoretical fits: red and light green – slopes of 5/9, light blue and pink – 5/6 and blue shows mixed behaviour, but further analysis shows that scaling is correct only for small displacements.

5. CONCLUSIONS

In a recent paper (Lovejoy *et al.* 2006), we proposed an anisotropic turbulence/wave model for the horizontal velocity and passive scalar fields. The model was an anisotropic, space-time, multifractal extension of the classical Kolmogorov and Corrsin-Obukhov laws, it was a turbulence/wave extension of the classical Fractionally Integrated Flux model. In (Lilley *et al.* 2004), we empirically verified the model by studying the horizontal-vertical stratification of passive scalars. This lead directly to the precise estimate for the elliptical dimension of the spatial structures: $D_s = 2.55 \pm 0.02$, which eliminates the main competing theories of stratification (with $D_s = 2, 7/3, 3$).

In this paper, we focused on the temporal behaviour; primarily the space-time stratification, but also the intermittency. The temporal scaling is more complex than the pure horizontal or vertical scaling treated in (Lilley *et al.* 2004) due to the effect of advection which leads to non-diagonal generators G . The consequences for (1D) time series is that there are in general three competing scalings with exponents $H = 1/3, 3/5, 1/2$ (corresponding to $\beta_\tau = 5/3, 11/5, 2$). The first two correspond to domination by horizontal and vertical advection, the third to “pure” temporal development. Surveying the literature, we again found support for the theory since many studies

found β_τ in the range $5/3 - 2$ (in addition, the main gravity wave theories agree about this).

In sections 3, 4, we again used lidar data - although this time of both aerosol and cirrus clouds - from six ground based lidar vertical-time cross-sections. We first confirmed the theoretical predictions in orthogonal (z, t) directions. In order to test the theory more generally (in non-orthogonal directions) and to more fully determine the physical scale function (the existence of which is the basic hypothesis of the FIF model), we developed a new Anisotropic Scaling Analysis Technique (ASAT) which we applied both in real and Fourier spaces. We compared the theoretically predicted behaviour to the data and showed good agreement between theory and experimental results over a wide range of space-time scales. As far as we could tell, the scaling of the cirrus clouds and aerosols were the same; they both followed the theoretical predictions of the turbulence/wave 29/9D space-time model.

Using this technique, we revisited some of the (x, z) cross-sections discussed in (Lilley *et al.* 2004) reconfirming the theory for non-orthogonal directions and determining the spatial part of the “symmetrized” scale functions. Due to this “symmetrization” and other factors, the measured scale function is not the same as the underlying physical scale function; hence we were unable to directly verify the wave extension to the classical FIF model.

Since in the FIF, an anisotropic physical scale is introduced to replace standard isotropic scales, it predicts that the anisotropies of the weak and strong structures are the same, hence it predicts constant ratios for structure function exponents in orthogonal directions. For the horizontal wind dominated cases we find the ratio $\xi_\tau / \xi_v = H_z = 0.54 \pm 0.02$ (theory predicts $H_z = 5/9 \approx 0.556$ and in (Lilley *et al.* 2004) a direct estimate gives $H_z = 0.55 \pm 0.02$) and for the pure temporal development case we found $\xi_\tau / \xi_v = H_z / H_t = 0.81 \pm 0.04$ (theory predicts $H_z / H_t = (5/9)/(2/3) = 5/6 \approx 0.833$), hence $H_t = 0.54/0.81 = 0.67 \pm 0.06$ or $H_t = 0.55/0.81 = 0.68 \pm 0.03$ depending on whether the empirical or theoretical H_z is used; theory predicts $2/3$. We conclude that the theory is confirmed to within experimental accuracy. This analysis gave us elliptical dimension in full space-time domain (x, y, z, t)

$$D_{st} \approx 1 + 1 + 0.54 + 0.67 = 3.21 \pm 0.06,$$

$$D_{st} \approx 1 + 1 + 5/9 + 0.68 = 3.24 \pm 0.03 \text{ that is very close to theoretical value of } 29/9.$$

If the analyses and models discussed here are correct in their essentials, then atmospheric dynamics are in many ways simpler than usually assumed, primarily because the 29/9D model unifies the dynamics over the entire dynamically significant range of space-time scales. Theoretically, this is compatible - if not demanded - by the dynamical equations which are scaling from planetary down to dissipation scales. All the competing models require on the contrary the existence of strong scale separations with the small and large scales interacting only weakly. This is true not only of the classical 2D-3D isotropic turbulence model, but also of the anisotropic gravity wave models which require a linearization of the dynamics about an ill defined reference state. The failure of modern data to corroborate the existence of a scale separation is probably the single most compelling argument in favour of the anisotropic scaling model; in this series, state-of-the-art lidar data quantitatively support the 29/9D model while excluding the competing 2D, 3D and 7/3D (gravity wave) models.

ACKNOWLEDGEMENTS

The authors would like to acknowledge the Meteorological Service of Canada for Pacific 2001 and CARE 2003 experiments. The authors also acknowledge the Center for Atmospheric Research Experiments for the close collaboration during this project and in particular the support of M. Travis. Shaun Lovejoy and Alexander Radkevich acknowledge the Canadian Foundation for Climate and Atmospheric Sciences for financial support.

REFERENCES

Balsley, B.B. and Carter, D.A. (1982), The spectrum of atmospheric velocity fluctuations at 8 km and 86 km, *Geophys. Res. Lett.*, **9**, 465.

Balsley, B.B. and Garello, R. (1985), The kinetic energy density in the troposphere, stratosphere and mesosphere: a preliminary study using the Poker Flat MST radar in Alaska, *Radio Sci.*, **20**, 1355.

Beatty, T.J., Hostetler C.A., and Gardner, C.S. (1992), Lidar observation of gravity waves and their spectra near the mesopause and stratopause at Arecibo, *J. Atmos. Sci.*, **49**, 477.

Dewan, E. 1997 Saturated-cascade similtude theory of gravity wave sepectra. *J. Geophys. Res.* **102**, 29799-29817.

Dewan, E. & Good, R. 1986 Saturation and the "universal" spectrum vertical profiles of horizontal scalar winds in the stratosphere. *J. Geophys. Res.*, **91**, 2742.

Fritts, D.C., Tsuda, T., VanZandt, T.E., Smith, S.A., Sato, T., Fukao, S., and Kato, S. (1990), Studies of velocity fluctuations in the lower atmosphere Using MU radar. Part II: Momentum flux and energy densities, *J. Atmos. Sci.*, **47**, 51.

Gagnon, J.S., S. Lovejoy, D. Schertzer, 2006: Multiscaling properties of the earth's topography from planetary to metric scales. Submitted to *J. Geophys. Res.*_(Earth Surface).

Gardner, C.S. and Voelz, D.G. (1987), Lidar studies of the nighttime sodium Layer over Urbana, Illinois 2. Gravity waves, *J. Geophys. Res.*, **92**, 4673.

Gardner, C. 1994 Diffusive filtering theory of gravity wave spectra in the atmosphere. *J. Geophys. Res.*, **99**, 20601.

Hwang H. J. (1970). Power Density Spectrum Of Surface Wind Speed On Palmyra Island. *Monthly Weather Review* **98**, 70

Inoue E. (1951). On the Turbulent Diffusion in the Atmosphere. *J. Met. Soc. Japan.*, **29**, 32.

Kwon, K.H., Gardner, C.S., Avery, S.K. and Avery, J.P. (1990), Correlative radar and sodium lidar observation of the vertical and horizontal structure of gravity waves near the mesopause, *J. Geophys. Res.*, **95**, 13737.

Landau L. D. and Lifshitz E. M. (1959). *Fluid Mechanics*, Pergamon, London, England.

Larsen, M.L., Kelly, M.C. and Gage, K.S. (1982), Turbulence spectra in the upper troposphere at periods between 2 hours and 40 days, *J. Atmos. Sci.*, **39**, 1035.

Lilley, M., Lovejoy S, Strawbridge K. and Schertzer D. (2004), 23/9 dimensional anisotropic scaling of passive admixtures using lidar aerosol data, *Phys. Rev. E*, **70**, 036307

Lilley, M., Lovejoy S, Strawbridge K., Schertzer D. and Radkevich A. (2006) Scaling turbulent atmospheric stratification, Part II: empirical study of the the stratification of the intermittency. Submitted to the *QJ Roy. Soc. Ref. # 05/230*

Lovejoy, S., Schertzer, D., Lilley, M., Strawbridge, K., and Radkevich A. (2006) Scaling turbulent atmospheric stratification, Part I: turbulence and waves. Submitted to the *QJ Roy. Soc. Ref. # 05/229*

Meek, C.E., Reid, I.M. and Manson, A.H. (1985), Observations of mesospheric wind velocities 2.

Cross sections of power spectral density for 48 – 8 hours, 8 – 1 hours, and 1 hour to 10 min over 60-110 km for 1981, *Radio Sci.*, **20**, 1383.

Radkevich A., Lovejoy, S., Strawbridge, K., Schertzer, D. (2006a) 29/9 dimensional space-time atmospheric stratification of passive admixtures using lidar data, Submitted to *Physica A*

Radkevich, A., Lovejoy, S., Strawbridge, K., Schertzer, D. and Lilley, M. (2006b) Scaling turbulent atmospheric stratification, Part III: : Space-time stratification of passive scalars from lidar data. Submitted to the *QJ Roy. Soc.* Ref. # 05/231

Scheffler, A.O. and Liu, C.H. (1985), On observation of gravity wave spectra in the atmosphere using MST radar, *Radio Sci.*, **20**, 1309.

Schertzer, D. & Lovejoy, S. (1983a) Elliptical turbulence in the atmosphere. In *forth symposium on turbulent shear flows*. Karlsruhe, West Germany.

Schertzer, D. & Lovejoy, S. (1985a) The dimension and intermittency of atmospheric dynamics. In *Turbulent Shear Flow 4* (ed. B. Launder), pp. 7-33: Springer-Verlag.

Schertzer, D. & Lovejoy, S. (1985b) Generalised scale invariance in turbulent phenomena. *Physico-Chemical Hydrodynamics Journal* **6**, 623-635.

Schertzer, D. & Lovejoy, S. 1987 Physical modeling and Analysis of Rain and Clouds by Anisotropic Scaling of Multiplicative Processes. *Journal of Geophysical Research* **92**, 9693-9714.

Schertzer, D., Schmitt, F., Naud, C., Marsan, D., Chigirinskaya, Y., Marguerit, C., and Lovejoy, S. (1998), New developments and old questions in multifractal cloud modeling, satellite retrievals and anomalous absorption, Proceedings of the 7th Atmos. Rad. Meas. (ARM) meeting, San Antonio, 1997.

Sica R. J. and Russell A. T. (1999). Measurements of the Effects of Gravity Waves in the Middle Atmosphere Using Parametric Models of Density Fluctuations. Part I: Vertical Wavenumber and Temporal Spectra. *J. Atmos. Sci.* **56**, 1308.

Strawbridge, K.B. and Snyder, B.J. 2004. Planetary boundary layer height determination during Pacific 2001 using the advantage of a scanning lidar instrument. *Atmos Environ.* **38** (34): 5861-5871.